

1 Development of a coupled current-wave model
2 to assess the impact of a hurricane on particle
3 transport

4 Thomas Dobbelaere, Emmanuel Hanert

5 February 9, 2021

6 **Abstract**

7 In most hydrodynamic model studies, currents and waves are simu-
8 lated separately. This is especially true for the simulation of passive
9 drifters, whose trajectories are often computed based solely on cur-
10 rents. Although this simplification holds for most situations, as the
11 force exerted by waves on currents can be neglected in fair weather
12 conditions, it may lead to significant errors in storm conditions, during
13 which local currents are strongly influenced by wind-generated waves.
14 In this study, current-wave interactions in heavy-wind conditions are
15 studied by coupling the unstructured-mesh hydrodynamic model SLIM
16 with the wave model SWAN in the Florida Reef Tract during Hurricane
17 Irma (Sep. 2017). This coupled model successfully reproduced both
18 the observed wave behavior and storm surge during the hurricane.
19 The modeled currents were then used to simulate the trajectories of
20 passive drifters during the passage of the hurricane. Our results show
21 that taking wave force into account induces variations of up 1 m/s
22 in modelled currents on the continental shelf break as well as in the
23 vicinity of reefs and islands. Wave-current interactions can therefore
24 strongly modify the transport of drifting material, such as sediments
25 and coral larvae, during heavy-wind events. That should in particular
26 affect connectivity modeling studies since coral mass spawning events
27 tend to occur during the hurricane season in the Caribbean.

²⁸ **1 Introduction**

²⁹ **2 Methods**

³⁰ **2.1 Wind and atmospheric pressure for Hurricane Irma**

³¹ In order to capture the wind speed profile of Irma in our model, high-
³² resolution H*Wind (Powell et al., 1998) wind fields were used. As these
³³ data represent 1-min averaged wind speeds, we multiplied them by a factor
³⁴ 0.93 to obtain 10-min averaged wind speeds (Harper et al., 2010), more
³⁵ consistent with the time step of our model. Pressure fields were obtained
³⁶ from ECMWF ERA-5 datasets. However, the coarse resolution of ERA-5
³⁷ caused the depression at the center of the hurricane to get smoothed out,
³⁸ leading to an underestimation of the pressure gradient in our model (see
³⁹ eq. 1). To better capture the central depression of Irma, we built a hybrid
⁴⁰ pressure field using the position and the minimal pressure of the core of
⁴¹ the hurricane based on its track in the HURDAT 2 database (Landsea and
⁴² Franklin, 2013). Based on this information, the hybrid pressure field was
⁴³ constructed by combining an idealized Holland pressure profile (Lin and
⁴⁴ Chavas, 2012) within the radius of maximum wind speed of Irma (Knaff et al.,
⁴⁵ 2018) with ERA-5 pressure field. The transition between from the Holland
⁴⁶ profile to ECMWF data outside the radius of maximum wind speed data was
⁴⁷ performed using a smooth step function.

⁴⁸ **2.2 Hydrodynamic model**

Ocean currents generated during hurricane Irma in the Florida Reef Tract (FRT) were modelled using the unstructured-mesh depth-integrated coast ocean model SLIM¹. The model mesh covers an area similar to the model extent of Dobbelaere et al. (2020), that includes the FRT but also the Florida Strait and part of the Gulf of Mexico (Figure 1). However, this area has been slightly extended northeastward and westward in order to include the location of buoys for wave outputs validation. Furthermore, in order to withstand potential cell drying due to storm conditions in this study, we used

¹<https://www.slim-ocean.be>

the conservative mode of SLIM with wetting-drying, whose equations write:

$$\begin{aligned} \frac{\partial H}{\partial t} + \nabla \cdot (\mathbf{U}) &= 0 \\ \frac{\partial \mathbf{U}}{\partial t} + \nabla \cdot \left(\frac{\mathbf{U}\mathbf{U}}{H} \right) &= -f \mathbf{e}_z \times \mathbf{U} + \alpha g H \nabla(H - h) - \frac{1}{\rho} \nabla p_{\text{atm}} + \frac{1}{\rho} \boldsymbol{\tau}_s \quad (1) \\ &\quad + \nabla \cdot (\nu \nabla \mathbf{U}) - \frac{C_b}{H^2} |\mathbf{U}| \mathbf{U} + \gamma (\mathbf{U}_* - \mathbf{U}) \end{aligned}$$

49 where H is the water column height and \mathbf{U} is the depth-averaged transport;
50 f is the Coriolis coefficient; g is the gravitational acceleration; h is the
51 bathymetry; α is a coefficient stating whether the mesh element is wet
52 ($\alpha = 1$) or dry ($\alpha = 0$); ν is the viscosity; C_b is the bottom drag coefficient;
53 ∇p_{atm} is the atmospheric pressure gradient; $\boldsymbol{\tau}_s$ is the surface stress due
54 to wind; and γ is a relaxation coefficient towards a reference transport \mathbf{U}_* .
55 As in Frys et al. (2020) and Dobbelaere et al. (2020), SLIM currents were
56 relaxed towards HYCOM (Chassignet et al., 2007) in regions where the water
57 depth exceeds a given threshold. At very high wind speeds, the white cap is
58 blown off the crest of the waves, which generates a layer of droplets that acts
59 as a slip layer for the winds at the ocean-atmosphere interface (Holthuijsen
60 et al., 2012). This causes a saturation of the wind drag coefficient for strong
61 winds (Donelan et al., 2004; Powell et al., 2003). To account for the impact
62 of this saturation on the surface wind stress in our model, we implemented
63 the wind drag parameterization of Moon et al. (2007).

64 The mesh resolution depended only on the distance to coastlines and reefs,
65 bathymetry and bathymetry gradient in order to satisfy SWAN refinement
66 criterion $h/A \geq a$, where h is the water depth and A is the element area.
67 The mesh was generated using the Python library seamsh², based on the
68 the open-source mesh generator GMSH (Geuzaine and Remacle, 2009) and
69 is composed of approximately 7.7×10^5 elements. The coarsest elements,
70 far away from the FRT, had a characteristic length size of about 5 km. Figure
71 1 depicts how a 100-m spatial resolution mesh simulated fine-scale details
72 of the ocean currents and significant wave height generated by hurricane
73 Irma in the Florida Keys.

²<https://pypi.org/project/seamsh/>

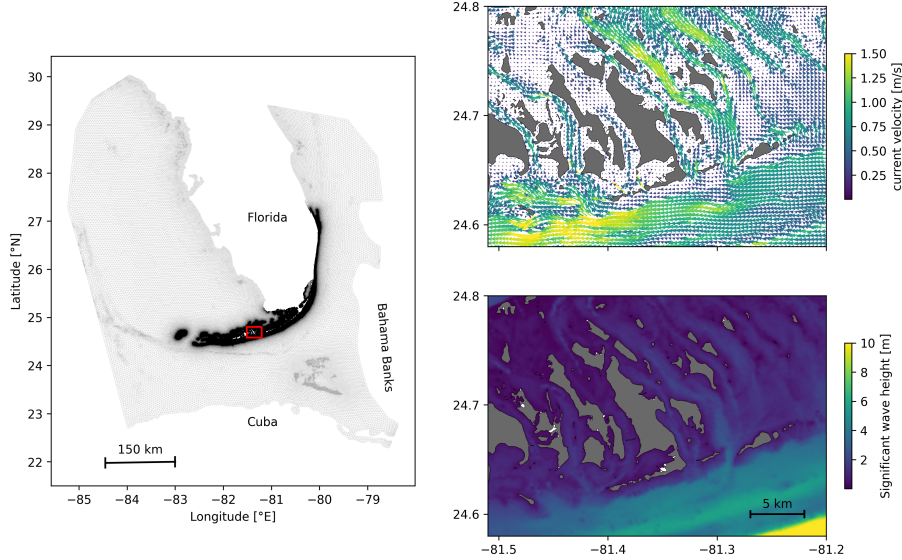


Fig. 1: Mesh of the computational domain with snapshots of simulated instantaneous currents and significant wave height on 2017-09-10 at 11:00:00. The mesh resolution ranges from 100 m in the Florida Keys to a maximum of 5 km offshore.

74 2.3 Wave model

Waves were modelled using parallel unstructured SWAN (Booij et al., 1999) on the same mesh as SLIM . This model solves the action balance equation, which reads (Mei, 1989):

$$\frac{\partial N}{\partial t} + \nabla_x \cdot [(c_g + \mathbf{u})N] + \frac{\partial}{\partial \theta}[c_\theta N] + \frac{\partial}{\partial \sigma}[c_\sigma N] = \frac{S_{in} + S_{ds} + S_{nl}}{\sigma} \quad (2)$$

where N is the wave action density; θ is the wave propagation direction; σ is the wave relative frequency; c_g is the wave group velocity, \mathbf{u} is SLIM depth-averaged current velocity; c_θ and c_σ are the propagation velocities in spectral space due to refraction and shifting in frequency due to variations in depth and currents; and S_{in} , S_{ds} , and S_{nl} respectively represent wave growth by wind, wave decay and nonlinear transfers of wave energy through interactions between triplets and quadruplets. Spectra were discretized with 48 direction bins and 50 frequency bins logarithmically distributed from 0.3 to 2 Hz. Exponential wind growth was parameterized using the formulation of Janssen (1991), while dissipations by whitecapping and bottom dissipations

followed the formulations of Komen et al. (1984) and Madsen et al. (1989) respectively. Coefficients for exponential wind growth and whitecapping parameterizations were based on the results of Siadatmousavi et al. (2011). Finally, wave boundary conditions were derived from WAVEWATCH III (Tolman et al., 2009) spectral outputs at buoy locations. Depth-averaged Stokes drift was also computed by SWAN using the following formula:

$$\mathbf{u}_s = \int_0^{2\pi} \int_0^{+\infty} \frac{\sigma^3}{h \tanh(2kh)} E(\sigma, \theta) (\cos \theta, \sin(\theta)) d\sigma d\theta \quad (3)$$

75 where k is the norm of the wave vector; h is the water depth; and $E(\sigma, \theta)$ is
 76 the wave energy density.

77 2.4 Coupled model

78 The coupling between SLIM and SWAN is illustrated in Figure 2. The two
 79 models are run consecutively at each time step. First, SLIM computes the
 80 sea surface elevation η and depth-averaged current velocity $\mathbf{u} = (u, v)$.
 81 These quantities are transferred to SWAN to update the model water depth
 82 as well as the second term of equation 2 governing wave energy propagation
 83 in the geographic space. Moreover, in order for the two model to have con-
 84 sistent bottom dissipation parameterizations, SLIM bottom drag coefficient is
 85 transformed into a roughness length z_0 following the methodology of Dietrich
 86 et al. (2011). This roughness length is then converted into Madsen's bottom
 87 dissipation term in SWAN . SWAN then produces the wave-induced force on
 88 current τ_{wave} by computing the wave radiation stress gradient. This quantity
 89 is used to update the value of the surface stress τ_s in equation 1, that now
 90 becomes the sum of wind and wave-induced forces $\tau_s = \tau_{\text{wind}} + \tau_{\text{wave}}$.

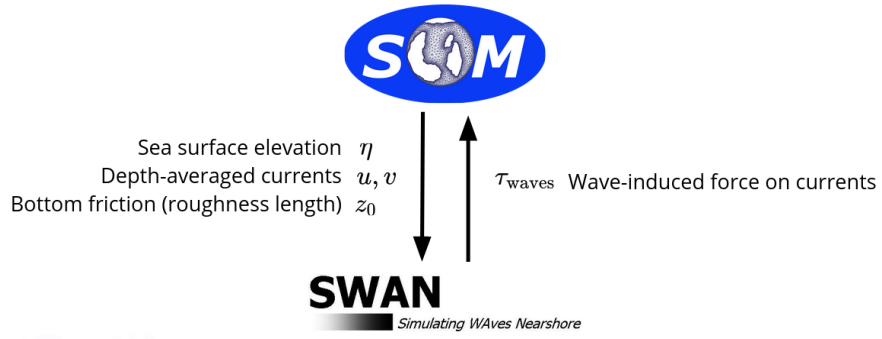


Fig. 2: Schematic illustration of the coupled SLIM +SWAN model.

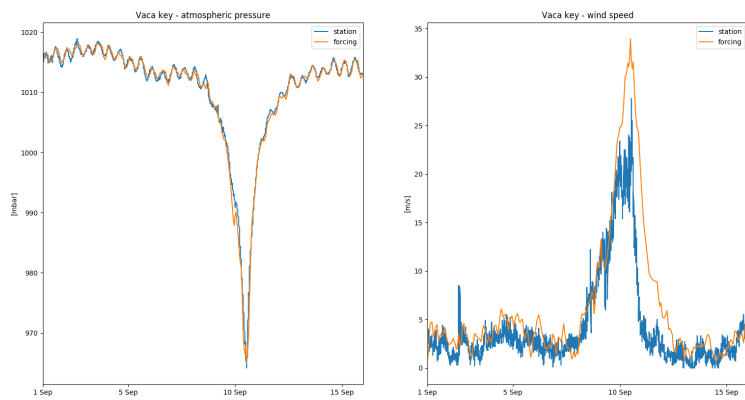


Fig. 3: The atmospheric forcings have been validated with meteorological station observations at Vaca Key. The reconstructed atmospheric pressure and wind speed agree well with field measurements.

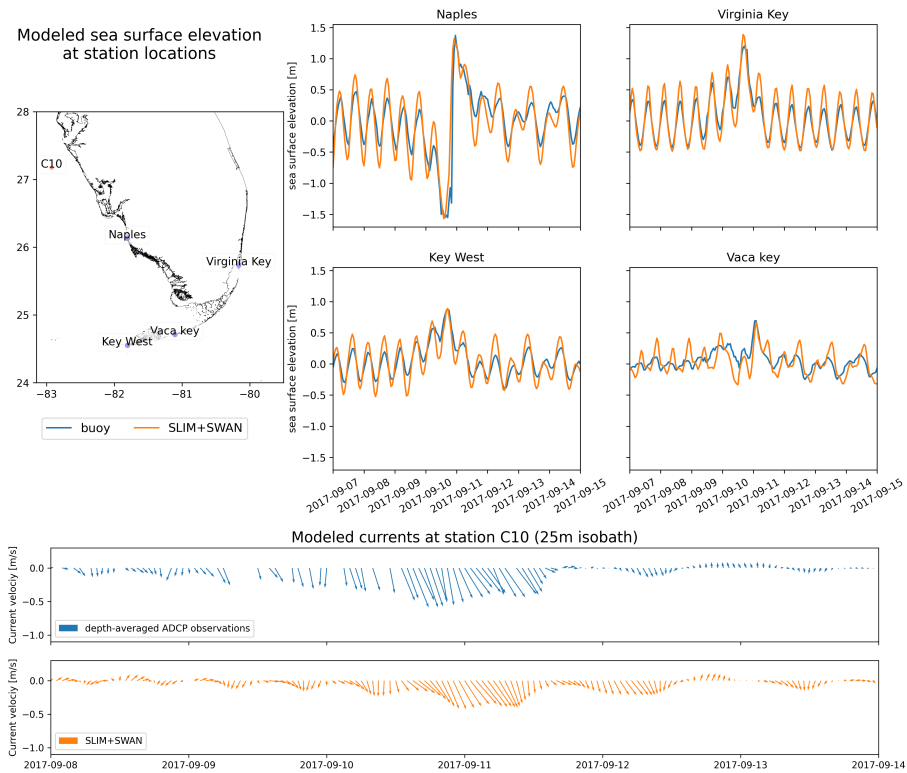


Fig. 4: The sea-surface elevation produced by the coupled wave-current model agrees with SSE and current velocity observations at different stations. The fit is particularly good in the Florida Keys and in Naples, on the inner Florida shelf. The coupled model currents have been validated against current meter data on the inner Florida shelf. The current speed and direction during the hurricane agrees well with the observations.

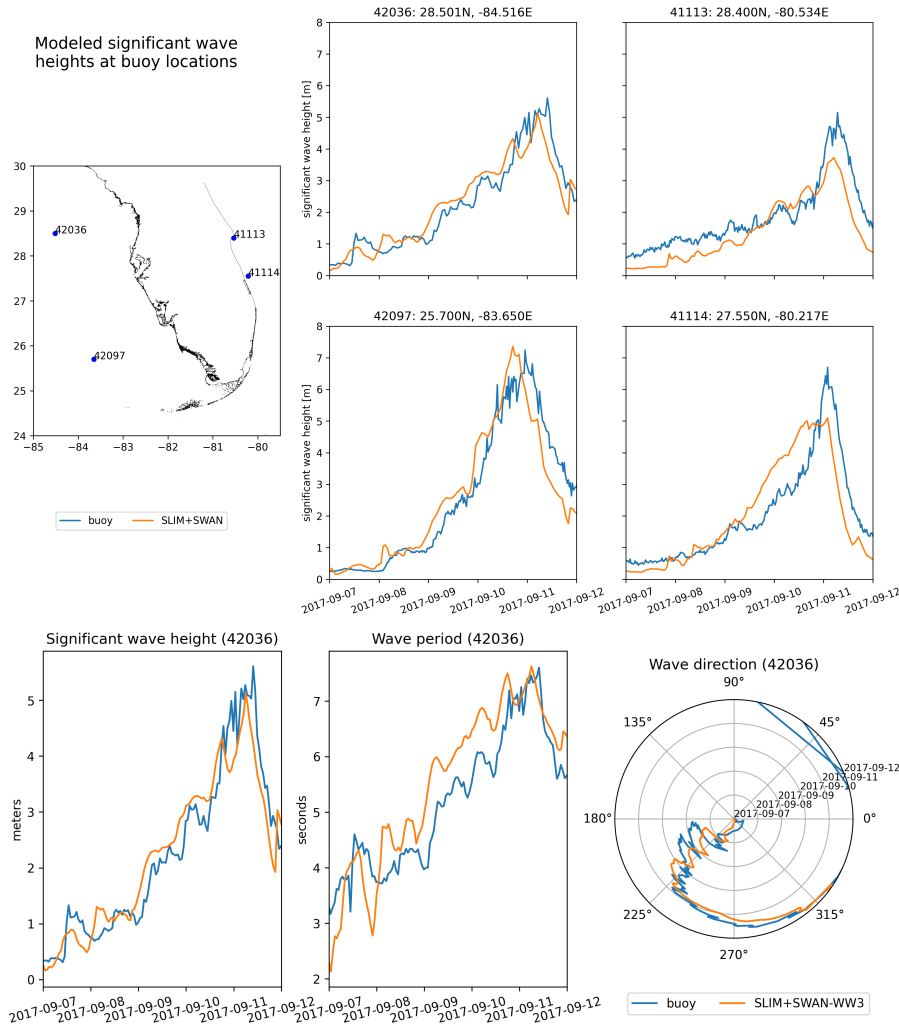


Fig. 5: The significant wave height produced by the coupled model has been compared to buoy measurements at 4 different stations. The timing and amplitude of the peak during the hurricane is correctly reproduced for all stations. For station 42036, the period and direction of the waves also agree well with observations

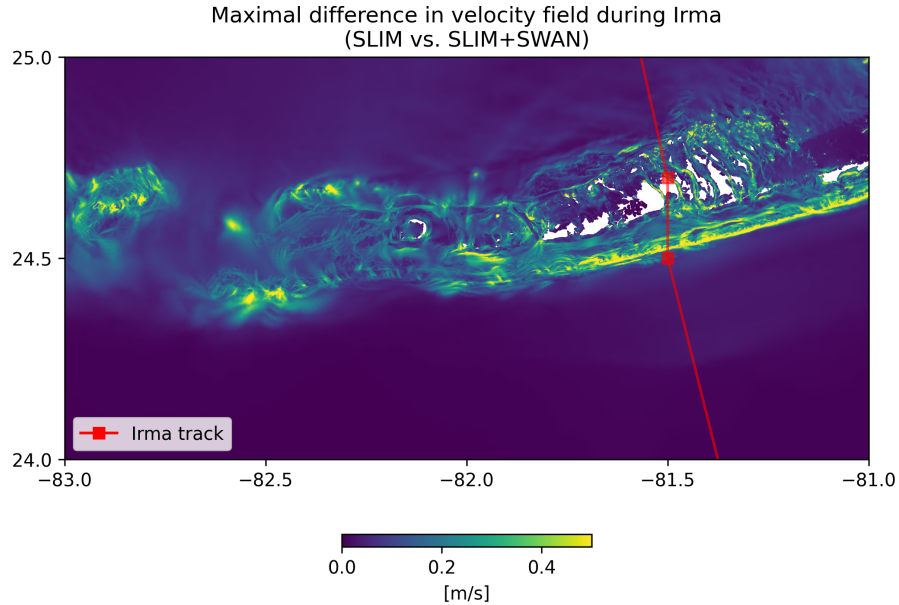


Fig. 6: Maximum of the difference between SLIM and SLIM+SWAN currents speed between 2017-09-07 00:00:00 and 2017-09-13 00:00:00. The difference between the coupled and uncoupled model, which represents the effect of the wave-induced stress, can yield differences of 0.5 m/s in the simulated currents during the passage of the hurricane. SLIM+SWAN currents velocities are larger than the currents modeled by SLIM alone.

91 **2.5 Comparison of particle trajectories**

92 **3 Results**

93 **3.1 Validation**

94 **3.2 Impact of waves**

95 **4 Discussion and conclusions**

96 Impact of waves on coral connectivity

97 Ability of wave model to correctly capture gradient in significant wave height
98 due to current-waves interactions under tropical cyclones depends on:

- 99 • Spatial (10km → 5km) and spectral (36 dir. → 48 dir.) resolution

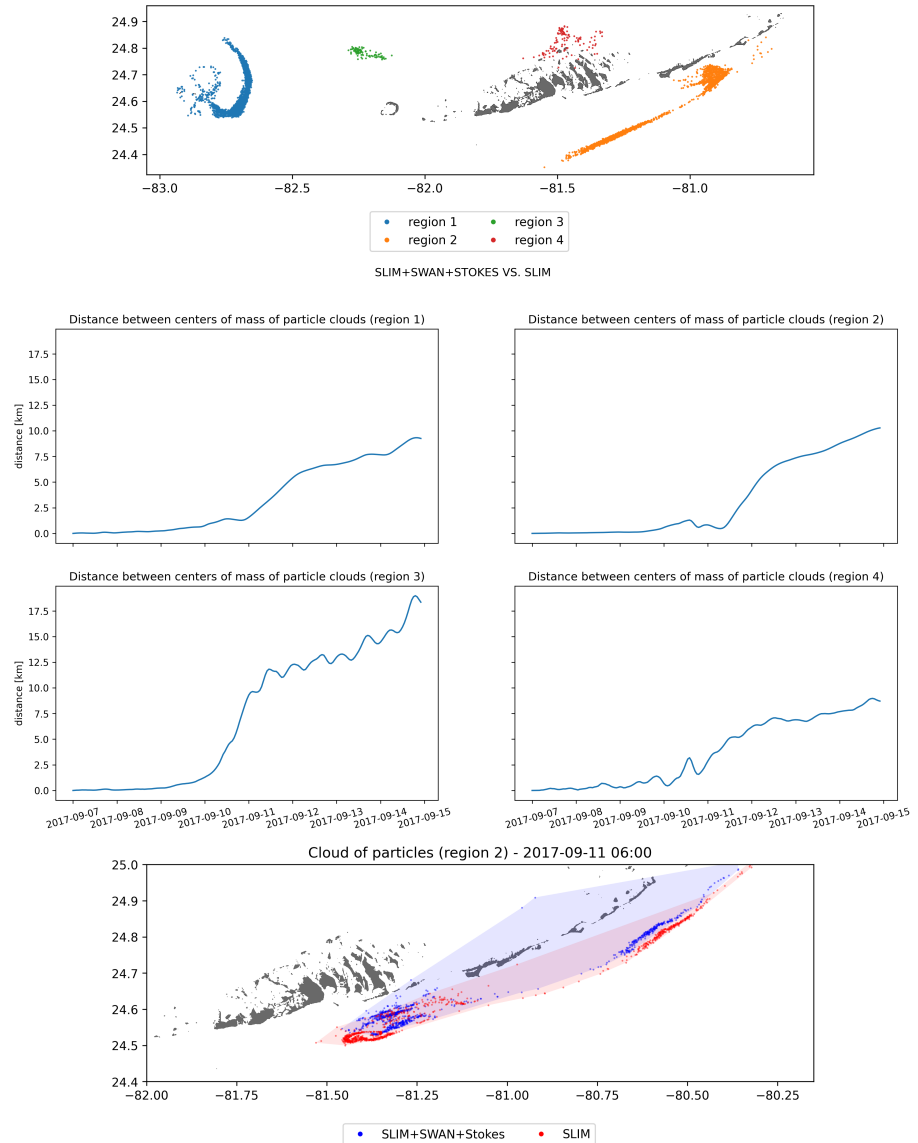


Fig. 7: Comparison of passive drifters trajectories with SLIM+SWAN+Stokes drift vs. SLIM alone. A snapshot of the positions of the particles released from region 2 is shown after the passage of Irma in the Florida Keys. Particles advected by the currents of the coupled model tend to remain on the shelf while particles advected by SLIM alone are mostly transported along the shelf break

¹⁰⁰ (Hegermiller et al., 2019)

- ¹⁰¹ • Directional spreading of incident waves (Villas Bôas et al., 2020)

¹⁰² **Conflict of Interest Statement**

¹⁰³ The authors declare that the research was conducted in the absence of any
¹⁰⁴ commercial or financial relationships that could be construed as a potential
¹⁰⁵ conflict of interest.

¹⁰⁶ **Author Contributions**

¹⁰⁷ **Funding**

¹⁰⁸ **Acknowledgments**

¹⁰⁹ Computational resources were provided by the Consortium des Équipements
¹¹⁰ de Calcul Intensif (CÉCI), funded by the F.R.S.-FNRS under Grant No. 2.5020.11.
¹¹¹ Thomas Dobbelaere is a PhD student supported by the Fund for Research
¹¹² training in Industry and Agriculture (FRIA/FNRS).

¹¹³ **Supplementary Material**

¹¹⁴ The Supplementary Material for this article is attached to the submitted
¹¹⁵ document.

¹¹⁶ **References**

¹¹⁷ Booij, N., Ris, R. C., and Holthuijsen, L. H. (1999). A third-generation wave
¹¹⁸ model for coastal regions: 1. Model description and validation. *Journal*
¹¹⁹ *of geophysical research: Oceans*, 104(C4):7649–7666.

- 120 Chassignet, E. P., Hurlburt, H. E., Smedstad, O. M., Halliwell, G. R., Hogan,
121 P. J., Wallcraft, A. J., Baraille, R., and Bleck, R. (2007). The HYCOM
122 (hybrid coordinate ocean model) data assimilative system. *Journal of*
123 *Marine Systems*, 65(1-4):60–83.
- 124 Dietrich, J., Westerink, J., Kennedy, A., Smith, J., Jensen, R., Zijlema, M.,
125 Holthuijsen, L., Dawson, C., Luettich, R., Powell, M., et al. (2011).
126 Hurricane gustav (2008) waves and storm surge: Hindcast, synoptic
127 analysis, and validation in southern Louisiana. *Monthly Weather Review*,
128 139(8):2488–2522.
- 129 Dobbelaere, T., Muller, E. M., Gramer, L. J., Holstein, D. M., and Hanert, E.
130 (2020). Coupled epidemi-hydrodynamic modeling to understand the
131 spread of a deadly coral disease in Florida. *Frontiers in Marine Science*,
132 7:1016.
- 133 Donelan, M., Haus, B., Reul, N., Plant, W., Stiassnie, M., Gruber, H., Brown,
134 O., and Saltzman, E. (2004). On the limiting aerodynamic roughness of
135 the ocean in very strong winds. *Geophysical Research Letters*, 31(18).
- 136 Frys, C., Saint-Amand, A., Le Hénaff, M., Figueiredo, J., Kuba, A., Walker, B.,
137 Lambrechts, J., Vallaeyns, V., Vincent, D., and Hanert, E. (2020). Fine-
138 scale coral connectivity pathways in the Florida Reef Tract: implications
139 for conservation and restoration. *Frontiers in Marine Science*, 7:312.
- 140 Geuzaine, C. and Remacle, J.-F. (2009). Gmsh: A 3-d finite element mesh
141 generator with built-in pre-and post-processing facilities. *International*
142 *journal for numerical methods in engineering*, 79(11):1309–1331.
- 143 Harper, B., Kepert, J., and Ginger, J. (2010). *Guidelines for converting*
144 *between various wind averaging periods in tropical cyclone conditions*.
145 Citeseer.
- 146 Hegermiller, C. A., Warner, J. C., Olabarrieta, M., and Sherwood, C. R.
147 (2019). Wave-current interaction between Hurricane Matthew wave
148 fields and the Gulf Stream. *Journal of Physical Oceanography*,
149 49(11):2883–2900.
- 150 Holthuijsen, L. H., Powell, M. D., and Pietrzak, J. D. (2012). Wind and waves
151 in extreme hurricanes. *Journal of Geophysical Research: Oceans*,
152 117(C9).

- 153 Janssen, P. A. (1991). Quasi-linear theory of wind-wave generation applied
154 to wave forecasting. *Journal of physical oceanography*, 21(11):1631–
155 1642.
- 156 Knaff, J. A., Sampson, C. R., and Musgrave, K. D. (2018). Statistical tropi-
157 cal cyclone wind radii prediction using climatology and persistence:
158 Updates for the western North Pacific. *Weather and Forecasting*,
159 33(4):1093–1098.
- 160 Komen, G., Hasselmann, S., and Hasselmann, K. (1984). On the exis-
161 tence of a fully developed wind-sea spectrum. *Journal of physical*
162 *oceanography*, 14(8):1271–1285.
- 163 Landsea, C. W. and Franklin, J. L. (2013). Atlantic hurricane database un-
164 certainty and presentation of a new database format. *Monthly Weather*
165 *Review*, 141(10):3576–3592.
- 166 Lin, N. and Chavas, D. (2012). On hurricane parametric wind and appli-
167 cations in storm surge modeling. *Journal of Geophysical Research: Atmo-*
168 *spheres*, 117(D9).
- 169 Madsen, O. S., Poon, Y.-K., and Gruber, H. C. (1989). Spectral wave
170 attenuation by bottom friction: Theory. In *Coastal Engineering 1988*,
171 pages 492–504.
- 172 Mei, C. C. (1989). *The applied dynamics of ocean surface waves*, volume 1.
173 World scientific.
- 174 Moon, I.-J., Ginis, I., Hara, T., and Thomas, B. (2007). A physics-based
175 parameterization of air–sea momentum flux at high wind speeds and
176 its impact on hurricane intensity predictions. *Monthly weather review*,
177 135(8):2869–2878.
- 178 Powell, M. D., Houston, S. H., Amat, L. R., and Morisseau-Leroy, N. (1998).
179 The HRD real-time hurricane wind analysis system. *Journal of Wind*
180 *Engineering and Industrial Aerodynamics*, 77:53–64.
- 181 Powell, M. D., Vickery, P. J., and Reinhold, T. A. (2003). Reduced drag coeffi-
182 cient for high wind speeds in tropical cyclones. *Nature*, 422(6929):279–
183 283.

- 184 Siadatmousavi, S. M., Jose, F., and Stone, G. (2011). Evaluation of two WAM
185 white capping parameterizations using parallel unstructured SWAN
186 with application to the Northern Gulf of Mexico, USA. *Applied Ocean*
187 *Research*, 33(1):23–30.
- 188 Tolman, H. L. et al. (2009). User manual and system documentation of
189 WAVEWATCH III TM version 3.14. *Technical note, MMAB Contribution*,
190 276:220.
- 191 Villas Bôas, A. B., Cornuelle, B. D., Mazloff, M. R., Gille, S. T., and Arduin,
192 F. (2020). Wave–current interactions at meso-and submesoscales:
193 Insights from idealized numerical simulations. *Journal of Physical*
194 *Oceanography*, 50(12):3483–3500.